Temperature-Responsive Polyelectrolyte Complexes for Bio-Inspired Underwater Adhesives

van Hees, Ilse A.; Hofman, Anton H.; Dompé, Marco; der Gucht, Jasper; Kamperman, Marleen

Published in:
European Polymer Journal

DOI:
10.1016/j.eurpolymj.2020.110034

Publication date:
2020

European Polymer Journal 141 (2020) 110034

Contents lists available at ScienceDirect

European Polymer Journal

journal homepage: www.elsevier.com/locate/europolj

Temperature-responsive polyelectrolyte complexes for bio-inspired underwater adhesives

Ilse A. van Hees[a], Anton H. Hofman[b], Marco Dompé[a], Jasper van der Gucht[a], Marleen Kamperman[b,*]

[a] Physical Chemistry and Soft Matter, Wageningen University and Research, Stippeneng 4, 6708 WE Wageningen, the Netherlands
[b] Polymer Science, Zernike Institute for Advanced Materials, University of Groningen, Nijenborgh 4, 9747 AG Groningen, the Netherlands

ARTICLE INFO

Keywords:
Wet adhesion
Polyelectrolyte complexation
Hydrophobicity
PNIPAM

ABSTRACT

Adhesive proteins of marine organisms contain significant amounts of hydrophobic amino acids. Therefore, inter- and intramolecular hydrophobic interactions are expected to play an important role in both adhesion and cohesion. Here, we mimic the hydrophobicity of adhesive proteins by using temperature-responsive polyelectrolyte complexes (TERPOCs) with a high poly(*N*-isopropylacrylamide) (PNIPAM) content. Upon mixing aqueous solutions of PNIPAM-*b*-poly(acrylic acid)-*b*-PNIPAM and poly(2-(dimethylamino) ethyl methacrylate) (PDMAEMA), complexation between the oppositely charged polyelectrolytes occurs. At low temperatures, complex coacervate core micelles (C3Ms) with a PNIPAM corona are formed, and upon a temperature increase, the solution turns into a hydrogel by the formation of a network of hydrophobic PNIPAM domains. Consequently, an abrupt increase in viscosity is observed upon heating which facilitates injectability of the adhesive. The gelation temperature, T_{gel}, and (adhesive) strength of the TERPOC can be adjusted by altering the salt and polymer concentration, which changes the balance between the electrostatic and hydrophobic interactions. Despite the importance of hydrophobic groups in strong underwater adhesives, we conclude that TERPOCs with a high PNIPAM content (70 wt%) are unstable due to water release. Consequently, there is a limited amount of hydrophobic groups that can be inserted in this type of systems. Nevertheless, TERPOCs show promising and tunable properties for application as injectable underwater adhesives, for example in biomedical applications.

1. Introduction

Adhesion is weakened by the presence of water, making underwater adhesion a technical challenge [1]. Nevertheless, in nature, several marine organisms adhere to slippery rocks or build protective shells underwater using adhesive proteins. A close look at the amino acid composition of the adhesive proteins used by these organisms reveals a high degree of hydrophobic, cationic and anionic amino acids [2].

Hydrophobic moieties can be beneficial for underwater adhesion in several ways. First, water has to be removed from the surface to enable proper binding between the substrate and the adhesive, and therefore increased hydrophobicity may facilitate contact formation [2]. Second, the presence of hydrophobic domains in a material reduces the water content and toughens the material, because the hydrophobic domains resist large deformations to minimize their contact with water [3]. Third, in several natural systems, complexation occurs between oppositely charged proteins, resulting in phase separation and formation of a complex coacervate [4]. This phase separation is promoted by hydrophobic groups through decreasing the solubility of the proteins in aqueous solution [2,5,6]. However, mimicking these features in synthetic systems is challenging because large amounts of hydrophobic moieties result in processing difficulties of water-based adhesives, i.e. the viscosity increase compromises injectability [7,8]. For this reason, we investigate the use of a temperature-responsive polymer, poly(*N*-isopropylacrylamide) (PNIPAM), to mimic the hydrophobic amino acids of the natural adhesive proteins without sacrificing the injectability.

PNIPAM is a well-studied temperature-responsive polymer with a lower critical solution temperature (LCST) [9]. Hence, PNIPAM is water-soluble at room temperature, but becomes insoluble when the LCST of approximately 32 °C is exceeded [10]. This change is induced by the formation of intramolecular hydrogen bonds, leading to a chain collapse and the formation of a water-insoluble material [11]. The use of PNIPAM in underwater adhesives allows easy processing below the

* Corresponding author.
E-mail address: marleen.kamperman@rug.nl (M. Kamperman).

https://doi.org/10.1016/j.eurpolymj.2020.110034
Received 6 July 2020; Received in revised form 11 September 2020; Accepted 14 September 2020
Available online 07 October 2020

LCST and solidification above the LCST [12–14].

To enhance and control the viscoelastic properties of the material, oppositely charged polyelectrolytes are inserted into the PNIPAM-based adhesive, which results in complexation. By adjusting the salt concentration, the viscoelastic properties of the complex can be tuned, which is a useful tool in the development of underwater adhesives. An increasing salt concentration will weaken the polyelectrolyte complex [15]. Moreover, weak polyelectrolytes have a pH-dependent degree of ionization. At low degrees of ionization, the polymers are more hydrophobic because of the uncharged moieties, leading to more solid complexes [3,16]. Finally, the degree of charge compensation (degree at which the polyelectrolyte charge is neutralized by oppositely charged polyelectrolytes) can be used to weaken or strengthen temperature-responsive polyelectrolyte complexes (TERPOCs). Excess charge can lead to changes in the material structure which results in different material properties.

Previous research has shown that hydrophobic surgical glues are particularly effective in wet environments. Karp et al. developed a hydrophobic pre-polymer (poly(glycerol sebacate acrylate) (PGSA)) which, after UV-crosslinking, showed stronger adhesion than commercially available tissue adhesives [17,18]. Others have shown that the combination of different types of non-covalent interactions may strongly increase adhesion [2]. For example, Waite and co-workers designed a high-performance mussel-inspired adhesive by combining catecholic, hydrophobic and electrostatic functional groups [19,20]. Moreover, several promising underwater adhesives were developed based on electrostatic interactions, but these adhesives contain considerably less hydrophobic compounds than natural underwater adhesives [2,12–14,21–23]. Therefore, we investigate the importance of hydrophobic interactions in complex coacervate-based underwater adhesives by using a PNIPAM content of 70 wt%. The adhesives are composed of a cationic homopolymer and an anionic triblock copolymer that contain large PNIPAM outer blocks. Upon mixing aqueous solutions of both components, the charged polymers electrostatically self-assemble into a charge-neutral complex. The use of well-defined linear polymers, allows us to obtain defined morphological features, as evidenced by small angle X-ray scattering.

In this work, TERPOCs are prepared by mixing PNIPAM-*b*-poly(acrylic acid)-*b*-PNIPAM ($NIPAM_{444}$-*b*-AA_{170}-*b*-$NIPAM_{444}$) and poly(2-(dimethylamino) ethyl methacrylate) ($DMAEMA_{680}$), Fig. 1. At low temperatures, the polyelectrolytes form complexes and stable complex coacervate core micelles (C3Ms) are obtained, Fig. 1C, resulting in a low viscosity polymer solution [24,25]. The insoluble polyelectrolyte core is stabilized by the long PNIPAM chains in the corona. Upon increasing the temperature, PNIPAM becomes insoluble resulting in gelation, and a TERPOC is formed, Fig. 1D. Gelation of the polymers provides cohesive strength to the TERPOC which is one of the main requirements for adhesive performance. This specific combination of polymers was chosen for several reasons. First, block copolymers are required to connect the PNIPAM and complex coacervate phases, which is expected to be important for the homogeneity of the TERPOC. The short anionic block was selected to maintain good control over the RAFT polymerization. At last, the large polycation was chosen to enable entanglement formation in the complex coacervate phase to enhance the strength of the TERPOC. The gelation temperature (T_{gel}), morphology, and adhesive strength of the TERPOC can be changed by altering the NaCl and polymer concentrations, as is observed by SAXS, rheology, and probe tack testing, respectively. Moreover, it is shown that charge neutralization is required for obtaining strong gels.

2. Experimental

2.1. Materials

Triethylamine (TEA) (⩾99%), propanethiol (99%), carbon disulphide (⩾99%), magnesium sulphate, 1,4-dioxane (99.8%), azobisisobutyronitrile (AIBN) (98%), *tert*-butyl acrylate (*t*BA) (98%) and aluminium oxide (neutral, Brockmann I) were purchased from Sigma Aldrich and used as received. *N*-isopropylacrylamide (NIPAM) (97%) was purchased from TCI. 1,4-bis(chloromethyl) benzene (BCMB) (98%), sodium chloride (> 99.5%) and hydrochloric acid (37%) were obtained from Acros Organics. Methanol (HPLC grade), 1,1,1,3,3,3-hexafluoro-2-propanol (HFIP) (AR), *n*-hexane (HPLC grade), dichloromethane (DCM) (AR), and diethylether (AR), were purchased from Biosolve and used as received. Sodium hydroxide solution (TitriPUR, 0.1 M) and hydrochloric acid (TitriPUR, 1 M) were bought from Merck chemicals. AIBN and NIPAM were recrystallized twice from methanol and *n*-hexane, respectively, and kept refrigerated before use. Furthermore, *t*BA was passed over a basic alumina column to remove inhibitor and used immediately.

$DMAEMA_{680}$ (M_n 107 kDa, Đ 1.26) was purchased from Polymer Source, Fig. S1.

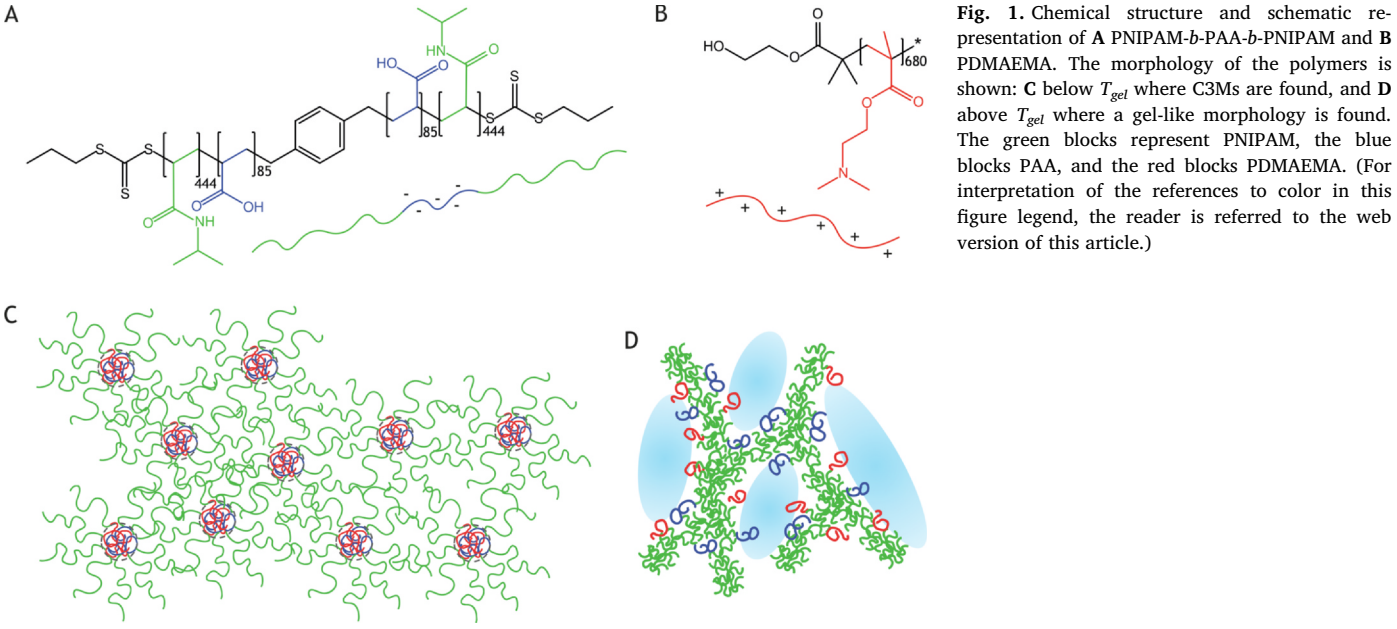

Fig. 1. Chemical structure and schematic representation of **A** PNIPAM-*b*-PAA-*b*-PNIPAM and **B** PDMAEMA. The morphology of the polymers is shown: **C** below T_{gel} where C3Ms are found, and **D** above T_{gel} where a gel-like morphology is found. The green blocks represent PNIPAM, the blue blocks PAA, and the red blocks PDMAEMA. (For interpretation of the references to color in this figure legend, the reader is referred to the web version of this article.)

2.1.1. Synthesis of divalent RAFT agent CDP

The chain transfer agent *C*,*C*'-[1,4-phenylenebis(methylene)] *C*,*C*'-dipropyl ester carbonotrithioic acid (CDP) was synthesized using an adapted method previously described by Bivigou-Koumba et al. [26] 2.6 g (34 mmol) carbon disulphide and 2.5 g (33 mmol) propanethiol were added to 10 mL chloroform and purged with nitrogen for 30 min. Subsequently, 3.5 g (35 mmol) TEA was added dropwise to the solution, resulting in a dark orange/yellow solution that evolved heat. The solution was left to stir for 30 min and subsequently 2.8 g (16 mmol) BCMB was added under nitrogen flow, again resulting in a warm solution. The solution was stirred overnight and subsequently diluted with 10 mL of chloroform, transferred to a separation funnel and washed thrice with 50 mL water. The organic layer was dried over magnesium sulphate and concentrated under reduced pressure. The resulting product was purified by recrystallization from DCM twice, and yielded a dark yellow solid, 5.8 g (90 %). ^{1}H NMR (400 MHz, $CDCl_3$, Fig. S2): δ (ppm) 1.03 (t, 6H, CH_3 propyl), 1.74 (sext, 4H, CH_2 propyl), 3.54 (t, 4H, CH_2 propyl), 4.60 (s, 4H, CH_2 methyl), 7.29 (s, 4H, benzyl) ppm. ^{13}C NMR (400 MHz, $CDCl_3$, Fig. S3): δ 13 (CH_3), 22 (CH_2 propyl), 39 (CH_2 thiol), 40 (CH_2 aryl), 130 (CH aryl), and 135 (C aryl) ppm.

2.1.2. Synthesis of PtBA from CDP

A round-bottom flask was loaded with 4.6 mg (0.028 mmol) AIBN, 230 mg (0.57 mmol) CDP, 15.5 g (121 mmol) *t*BA, and 44 mL dioxane (i:R:m as 0.05:1:210, [m] 2 M). The clear yellow solution was purged with nitrogen for 60 min. The polymerization took place for 5 h at 70 °C, and a conversion of 80% was reached. The reaction was quenched by exposure to air and rapid cooling. The polymer was purified by precipitation into a cold 3/1 (v/v) methanol/water mixture three times. The product was obtained as a yellow powder by drying in a vacuum oven and yielded 10 g (83%). ^{1}H NMR (400 MHz, $CDCl_3$): δ 1.4 (s, 9H, $(CH_3)_3$ *tert*-butyl), 1.6–2.3 (m, backbone) ppm, M_n 21.5 kDa. GPC (HFIP): M_n 22.0 kDa, Đ 1.25.

2.1.3. Synthesis of PNIPAM-b-PtBA-b-PNIPAM from CDP-functionalized PtBA

In a round-bottom flask 1.6 mg (0.0097 mmol) AIBN from a stock solution, 4.0 g (0.18 mmol) P*t*BA and 28.1 g (248 mmol) NIPAM were dissolved in 100 mL dioxane (i:R:m as 0.05:1:1250, [m] 2 M). The reactants were dissolved and the mixture was purged with nitrogen for 150 min. The polymerization was allowed to run for 6 h at 70 °C, till a conversion of 65% was reached. Subsequently, the reaction was quenched by cooling the reaction mixture rapidly and exposing it to air. The resulting polymer was purified by precipitation into a 4/1 (v/v) *n*-hexane/diethyl ether mixture for five times. The final product was dried in a vacuum oven to yield 17 g white powder. ^{1}H NMR (400 MHz, MeOD): δ 1.17 (s, 6H, $(CH_2)_2$ isopropyl), 1.49 (s, 9H, $(CH_3)_3$ *tert*-butyl), 1.55–2.3 (m, backbone), 3.98 (s, 1H, CH isopropyl) ppm, M_n 92.0 kDa, 81 mol% PNIPAM. GPC (HFIP): M_n 61.6 kDa and Đ 1.61.

2.1.4. Deprotection of PNIPAM-b-PtBA-b-PNIPAM

The resulting block copolymer was deprotected by dissolving 6 g in 140 mL HFIP, containing 0.1 M hydrochloric acid (1.8 equivalent) and the mixture was left to stir for 5 h at room temperature [27]. The sample was dried using rotary evaporation, redissolved in water and neutralized by using 1 M sodium hydroxide solution. The final product was obtained after freeze drying. ^{1}H NMR (400 MHz, MeOD): δ 1.16 (s, 6H, $(CH_3)_2$ isopropyl), 1.55–2.3 (m, backbone), 3.97 (s, 1H, CH isopropyl).

2.2. Methods

2.2.1. Sample preparation

The polymers were dissolved in water as stock solutions with a concentration of max. 12.5 wt% and the pH was adjusted to 6.5±0.2 to obtain an equal charge density for both PAA and PDMAEMA [6]. Samples were prepared by mixing the polycation with the NaCl solution, followed by the addition of the polyanion. The solution was vortexed and left refrigerated to equilibrate. Then, the pH was checked and adjusted to 6.5 ± 0.2 using 1 M NaOH or HCl. Finally, water was added to obtain the desired concentration, and the samples were kept refrigerated until further use. The order of mixing the polyelectrolytes is important as it determines the degree of coacervation. Moreover, the polymers were mixed in such a ratio that a charge-neutral complex was obtained and complexaxtion was maximized. Charge stoichiometry was verified by zeta potential measurements that should give values of about 0 mV. While being dependent on both the salt concentration and pH, the ionization degree of both polyelectrolytes is estimated to be higher than 90% [6]. The samples are prepared below the critical salt concentration ($c_{s,cr}$) of this polyelectrolyte pair, Fig. S12.

2.2.2. SAXS

Small-angle X-ray scattering (SAXS) measurements were carried out at the Dutch-Belgian Beamline (DUBBLE) station BM26B of the European Synchrotron Radiation Facility (ESRF) in Grenoble, France [28,29]. The sample-to-detector distance (Dectris Pilatus 1 M) was ca. 2.5 m. The scattering vector q is defined as $q = 4\ \pi/\lambda\ \sin(\theta)$ with 2θ being the scattering angle and λ the wavelength of the X-rays (1.03 Å). Silver behenate was used to calibrate the q-range, which covered 6.05 * 10^{-2} to 3.66 nm^{-1}. Two-dimensional images were radially averaged around the centre of the primary beam to obtain the isotropic SAXS profiles. The data was corrected for absorption and background scattering of the salt solutions. The samples were placed in a 2 mm quartz capillary and heated from 10 to 50 °C taking steps of 2–5 °C, with the temperature kept constant after each step for five or ten minutes, Table S1. The acquisition time was 30 s per frame. Every second-last frame of each temperature step was taken for analysis.

2.2.3. Rheology

Rheological measurements were performed on an Anton Paar MCR 301 rheometer equipped with a 25 mm cone-plate geometry. The temperature was controlled using a Peltier element. After making contact with the cone, the sample was immersed in tetradecane oil to avoid evaporation of water from the sample. First, the samples were equilibrated for 1 h at 10 °C, then the temperature was increased from 10 to 50 °C with 0.13 °C/min, followed by another equilibration for 2 h at 50 °C. During these steps the sample was measured using an oscillatory shear with 1% strain, and an angular frequency of 1 rad/s. After temperature increase, either shear start-up experiments were performed using a rotation with a fixed shear rate of 0.1 s^{-1}, or frequency sweeps were measured using an oscillation with 1% strain, and angular frequencies of 0.1 to 100 rad/s.

2.2.4. Probe tack testing

Adhesion tests were performed by using the probe tack method using an Instron 5333 materials testing system equipped with a 10 N load cell. A parallel contact and detachment between glass and the TERPOCs was made. In detail: A stainless steel probe, with a glass slide attached, was fixed onto the load cell. The polymer solution was pipetted onto a glass slide which subsequently was fastened to the bottom of the chamber using plastic screws. Contact between the clean glass slide and the polymer solution was made at 20 °C until a thickness of 0.5 mm was reached. Then, a 50 °C aqueous NaCl solution, with the same salt concentration as the polymer solution, was poured into the chamber and kept at this temperature. Thereafter, the probe was kept at a fixed distance from the glass surface for 1 min, followed by detachment at a fixed strain rate of 0.2 s^{-1}. Raw data of force and displacement were converted into stress and strain values to obtain the work of adhesion. The strain ϵ was obtained by normalizing the displacement by the initial thickness of the sample (t_0). The normalized stress σ was obtained by dividing the force by the contact area. The work of adhesion W_{adh} was calculated using Eq. 1

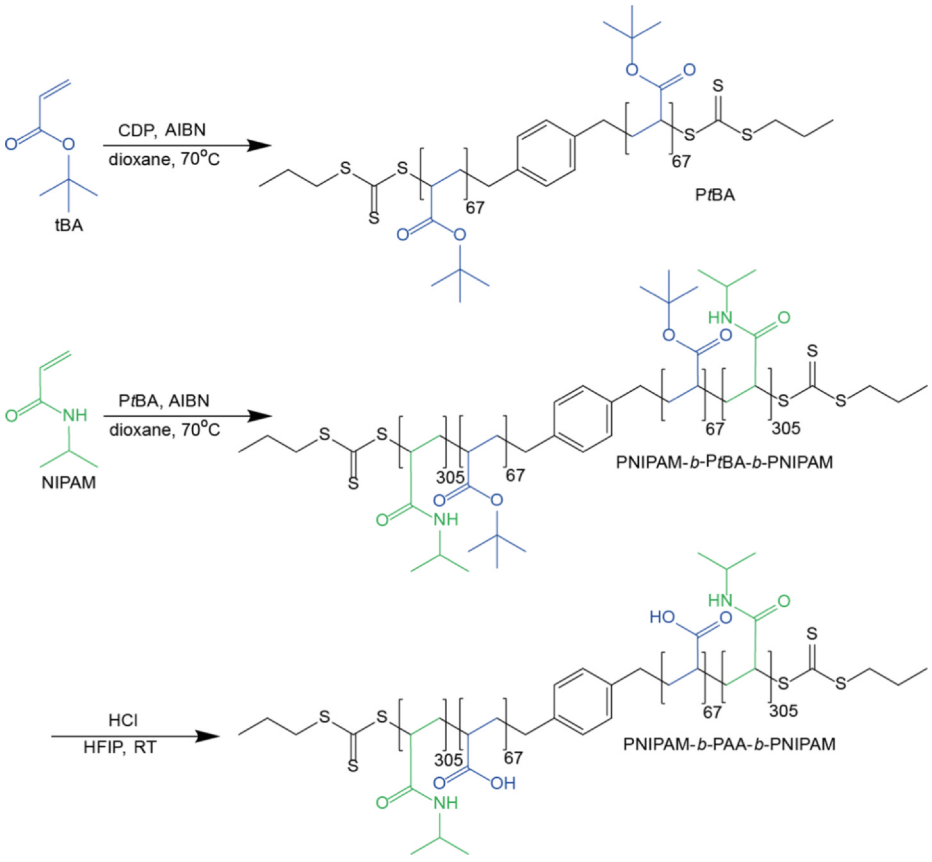

Scheme 1. Reaction scheme for the synthesis of PNIPAM-*b*-PAA-*b*-PNIPAM from RAFT-agent CDP. At first the P*t*BA macro-CTA is synthesized, followed by the copolymerization with NIPAM to yield PNIPAM-*b*-P*t*BA-*b*-PNIPAM. Subsequently the *tert*-butyl groups are removed under acidic conditions to yield PNIPAM-*b*-PAA-*b*-PNIPAM.

$$W_{adh} = t_0 \int_0^{\epsilon_{max}} \sigma d\epsilon \quad (1)$$

Two or three replicates were conducted for every experiment to ensure data reproducibility, and the work of adhesion is calculated using two measurements.

3. Results and discussion

3.1. Polymer synthesis

The PNIPAM-*b*-PAA-*b*-PNIPAM copolymer was synthesized using the divergent RAFT agent CDP, Scheme 1. First, the P*t*BA macro-CTA was synthesized, followed by a copolymerization with NIPAM to obtain the BAB triblock copolymer. The GPC traces of the macro-CTA and the block copolymer are shown in Fig. 2A and B, and are measured in HFIP. It can be seen that the peak of the P*t*BA is narrow and highly symmetric (Đ 1.25) and similar M_n values are obtained from NMR. These observations indicate that CDP provided good control over the polymerization of *t*BA and that termination was negligible. The signal of the PNIPAM-*b*-P*t*BA-*b*-PNIPAM copolymer shifted to lower retention volumes and broadened, with a Đ of 1.61. The GPC-peak has a small shoulder at higher retention volumes, indicating the presence of a minor amount of shorter chains. As the shoulder does not overlap with the P*t*BA macro-CTA, it can be concluded that all P*t*BA chains are extended. The smaller polymers can therefore be terminated block copolymers, or PNIPAM homopolymers, which can be caused by the high degree of polymerization of NIPAM. From GPC, an M_n of 17.6 kDa (DP 134) was measured for P*t*BA. From the integrals in the NMR, Fig. 2C, a NIPAM degree of polymerization of 610 is calculated, leading to a M_n of 86.8 kDa for the PNIPAM-*b*-P*t*BA-*b*-PNIPAM. As a result, the polymer has 82 mol% NIPAM over *t*BA.

After successful synthesis of PNIPAM-*b*-P*t*BA-*b*-PNIPAM, the block copolymer was converted into PNIPAM-*b*-PAA-*b*-PNIPAM by cleaving the *tert*-butyl groups in HFIP under acidic conditions at room temperature. The more commonly used and slower TFA/DCM method results in incomplete deprotection of PNIPAM-*b*-P*t*BA-*b*-PNIPAM, i.e. yields polymers that still contain small amounts of *t*BA, as was reported by Filippov et al. [27]. These small amounts of hydrophobic *t*BA were found to significantly affect the viscosity of PNIPAM-*b*-PAA-*b*-PNIPAM in water. As our triblock copolymers are prepared for application in aqueous solution, the *t*BA groups should be removed quantitatively, as is confirmed by the complete disappearance of the *tert*-butyl peaks, Fig. 3.

3.2. SAXS

SAXS experiments are performed to determine the morphology of the polymers both in solution and in the TERPOC at various salt and polymer concentrations (Figs. S4 and S5). First, the scattering curves of all samples at 10 °C will be discussed. Subsequently, the changes induced by increasing the temperature from 10 to 50 °C are explained, and, finally, the scattering curves at 50 °C are compared.

At 10 °C, PNIPAM is soluble, while the polyelectrolytes can form complex coacervates. In previous work we have shown that under these conditions C3Ms with a polyelectrolyte core and PNIPAM corona are formed [24]. Therefore, scattering peaks in the SAXS profiles are most likely caused by the complex coacervate cores. At low salt concentrations, two or three peaks can be observed, while at high salt concentration only a broad peak is detected, Fig. 4A [30]. The two peaks at low q values are assigned to be structure peaks, and are used to determine the morphology. For 0.3 M NaCl, the two structure peaks are located at 0.16 nm^{-1} and ≈ 0.26 nm^{-1}, and the ratio between these q values is 1.63 which is close in value to $\sqrt{8/3}$ and $\sqrt{3}$. Generally, spheres in a face-centred cubic (fcc) lattice display a second order peak at $\sqrt{4/3}$ q^* and a more intense third order peak at $\sqrt{8/3}$ q^* [31,32]. Therefore, it can be that the peak at 0.26 nm^{-1} is a third order peak of

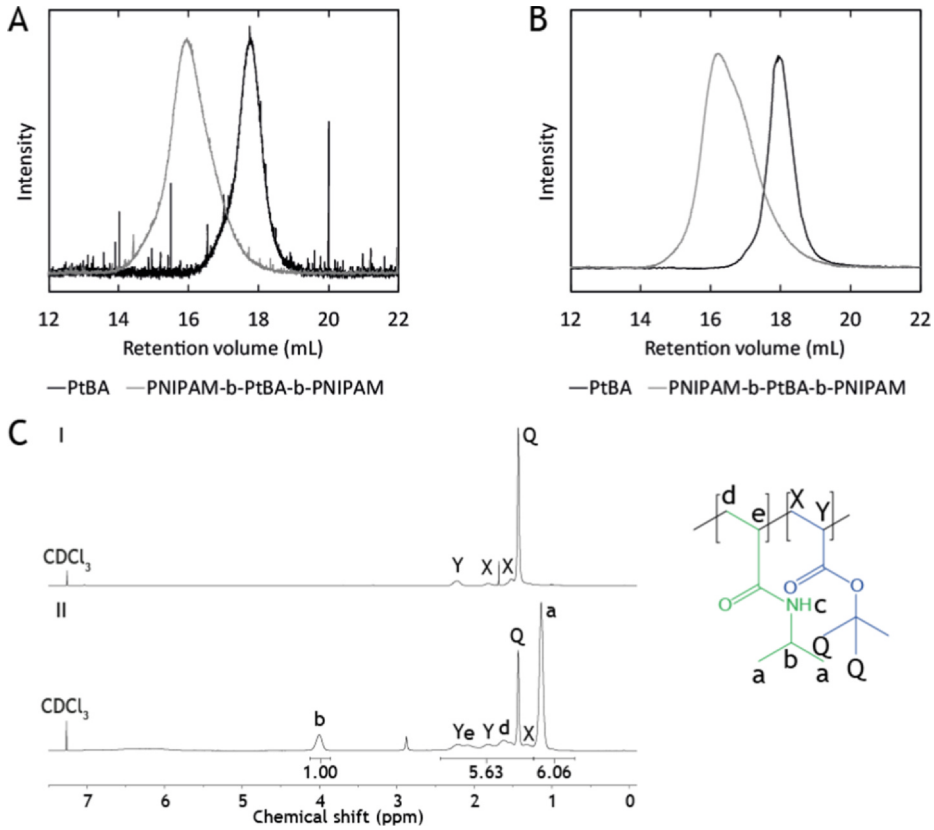

Fig. 2. HFIP GPC traces from **A** the light scattering and **B** the RI signal. The intensities of the GPC curves are normalized to the maximum detector response. **C** ^{1}H NMR in $CDCl_3$ of the P*t*BA macro-CTA (I), and PNIPAM-*b*-P*t*BA-*b*-PNIPAM (II).

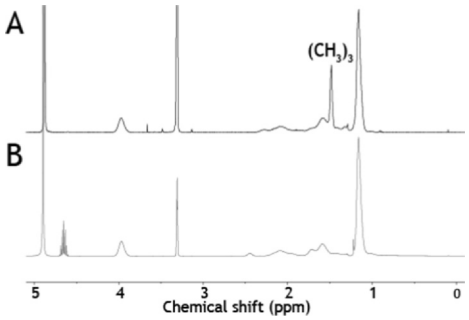

Fig. 3. ^{1}H NMR in MeOD of **A** PNIPAM-*b*-P*t*BA-*b*-PNIPAM and **B** PNIPAM-*b*-PAA-*b*-PNIPAM.

an fcc lattice with a spacing of ≈40 nm, while the second order peak is not visible. However, a body-centred cubic (bcc) lattice, is characterised by a second order peak at $\sqrt{3}$. Moreover, also non-crystalline samples can show a second order peak. Consequently, it remains unclear if ordering is present due to the broadness of the second structure peak.

Upon increasing the salt concentration, the structure peaks shift to higher *q*, indicating smaller domain spacing. This can be explained by the fact that the solubility of PNIPAM decreases with increasing salt concentration which results in a smaller occupied volume, thereby decreasing the distance between the complex coacervate domains [33,34]. Moreover, the peaks broaden with increased salt concentration which can be caused by either loss of contrast or loss of order. At higher salt concentrations, the complex coacervate core swells, while the PNIPAM corona shrinks, which reduces the contrast between the two phases. In addition, the lower mobility of the PNIPAM chains at higher salt may hinder equilibration and reduce the order in the sample, leading to peak broadening. The structure peaks also shift as function of the polymer concentration, Fig. 4B. For higher polymer concentrations, q^* moves to higher *q* values, as is seen for 7.5 and 10 wt% polymer. As reported before, the interdomain spacing depends on the polymer concentration, and decreases with increasing concentration [35]. For 4 wt% polymer, however, only a broad peak can be observed which is caused by loss of order which occurs at low polymer concentrations when micelles are too far apart to pack in a regular arrangement [31].

Upon increasing the temperature, several changes can be observed, Fig. 4C. First, the structure peak shifts to higher *q* values, indicating a decrease in the interdomain distance, which is a result of the shrinking PNIPAM corona and changing morphology [33,34]. Second, the structure peaks broaden which is clearly seen when comparing the scattering curves of 10 and 24 °C. Peak broadening indicates loss of contrast between core and corona, or loss of long range order due to a changing morphology [36]. Finally, the slope of the scattering curves at low *q* values increases from 26 °C onwards, which indicates the formation of aggregates in the samples, illustrating the gelation of the material [37]. This is in agreement with previously published work where it was shown that the LCST of PNIPAM decreases with increasing salt and polymer concentration [38,39].

At 50 °C, a broad shoulder can be observed for the samples with 7.5 wt% polymer, Fig. 5A. With increasing concentrations of NaCl, it can be seen that the width of the shoulder decreases, and the onset of the shoulder shifts to higher *q* values. This shift can again be explained by salt-induced deswelling of the PNIPAM, leading to lower interdomain spacing [33,34]. At 0.3 M NaCl and 10 wt% polymer, Fig. 5B, no broad shoulder, but two small peaks are observed. No distinct pattern can be discovered in the peak positions at low q and the indicated peaks. Therefore, we conclude that the material is most likely in a disordered state.

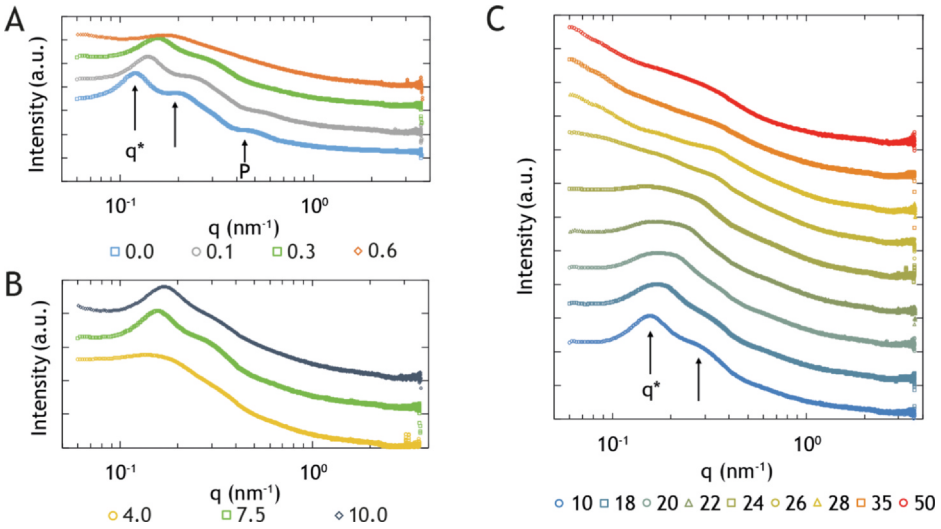

Fig. 4. A Scattering profiles with varying NaCl concentration (M) and 7.5 wt% polymer at 10 °C. The structure peaks are indicated with the arrows, and the form factor peak is indicated with P. **B** Scattering profiles with varying polymer concentration (wt%) and 0.3 M NaCl at 10 °C. **C** Scattering profiles of 0.3 M NaCl and 7.5 wt% polymer with increasing temperature (°C) (from bottom to top), for clarity temperatures at which no changes occurred have been left out. The curves are shifted over the y-axis for a better visibility.

3.3. Rheology

Rheology is used to determine the mechanical properties of the polyelectrolyte complexes and to study the gelation of the micellar solution. Here, it is discussed how the linear rheology (Fig. S7), as characterized by T_{gel}, G', G'', tan δ, and the non-linear rheology are affected by different NaCl, polymer, and PNIPAM concentrations, as well as different degrees of charge neutralization.

3.3.1. Salt dependence

In this section, the temperature-dependent behaviour of 7.5 wt% polymer solutions at three different salt concentrations is presented. The polymer concentration is varied in a later stage.

Temperature sweep. Fig. 6A shows the gelation of the micelle solution while increasing the temperature. At low temperatures, G'' exceeds G' indicating fluid-like materials. Moreover, at these temperatures, the viscosity is so low that G' and G'' are close to the detection limit of the rheometer. When the temperature increases, the moduli increase and a cross-over between G' and G'' is observed at T_{gel}. This cross-over indicates the gelation of the polymer solution which is induced by the LCST of PNIPAM. Following the cross-over, a further increase of G' and G'' is observed, and finally plateau moduli are found at 50 °C. From this pattern, it becomes evident that the temperature response is an abrupt transition from fluid to solid, which is an important feature for the injectability of adhesives. Furthermore, in Fig. 6, it is seen that the temperature-induced changes in the moduli occur at lower temperatures for higher salt concentrations. Affirmingly, it is known that the LCST of PNIPAM decreases linearly with increasing NaCl concentrations, which decreases T_{gel} [11,24,39]. Hysteresis between the moduli is observed, Fig. S7, upon measuring a temperature loop in which a temperature decrease follows upon a temperature increase. This hysteresis indicates a slow equilibration of the TERPOCs, as is discussed in the supplementary information [47–50]. Moreover, samples with less than 0.3 M NaCl show a cross-over of the moduli when increasing the temperature, but the increase of the moduli is unstable, Fig. S8 A. This instability results from wall-slip caused by the expulsion of water upon gelation. Expulsion of water and phase separation are undesired processes for underwater adhesives as contact with the substrate will be lost. For this reason, the separate components of the TERPOC (PNIPAM or polylectrolyte complexes) are unsuitable as adhesives by themselves, because phase separation occurs upon heating and at low salt concentrations respectively, Figs. S8 B and S12.

Fig. 6B indicates that the storage modulus at 50 °C, decreases slightly with increasing salt concentration. This is the result of the counteracting influence of salt on the electrostatic and hydrophobic interactions. Increasing salt concentrations lower the strength of the electrostatic interactions, thereby decreasing G' [6,16]. However, increasing salt concentrations lower the solvent quality of PNIPAM, leading to stronger intermolecular interactions. As a result, the contribution of PNIPAM to G' increases. Consequently, only a minor decrease in G' is observed, which clearly shows that the properties of TERPOCs are based on a balance between the electrostatic and

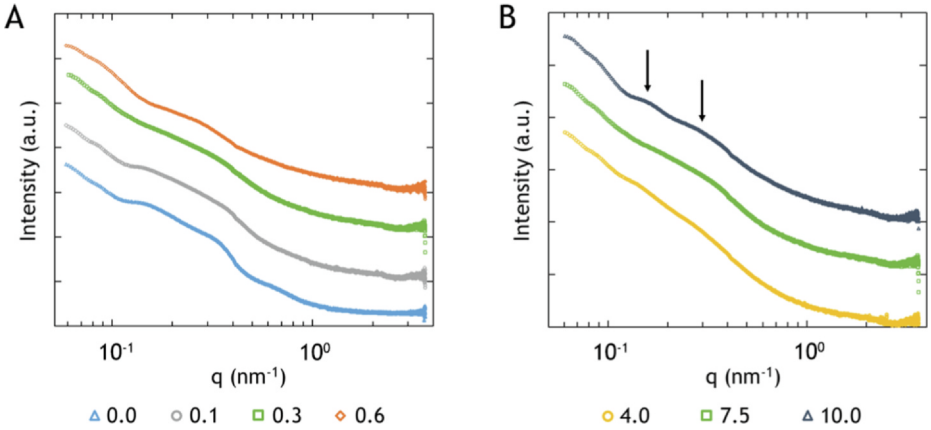

Fig. 5. A Scattering profiles with changing NaCl concentration (M) at 7.5 wt% polymer at 50 °C. **B** Scattering profiles with changing polymer concentration (wt%) at 0.3 M NaCl and 50 °C.

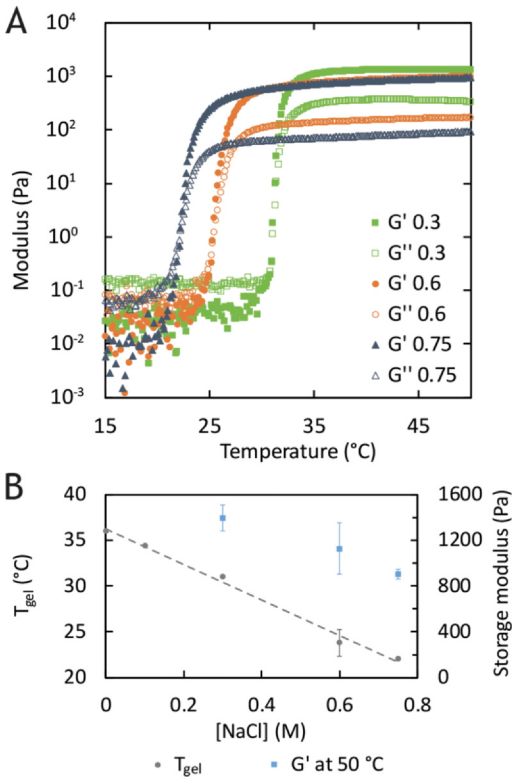

Fig. 6. A Storage and loss moduli at 1 rad/s as a function of temperature, for varying NaCl concentrations (M) at 7.5 wt% polymer. **B** *G'* as obtained at 50 °C before equilibration, and T_{gel} as determined from the cross-over temperature, are shown as function of NaCl concentration. The standard deviations are indicated by error bars. Except for 0.0 and 0.1 M NaCl, all samples have been measured multiple times. The temperature sweeps of 0.0 and 0.1 M NaCl can be found in Fig. S8.

Table 1
Tan δ as determined from the ratio between the loss (*G''*) and storage modulus (*G'*). All samples contained 7.5 wt% polymer and were measured at 50 °C.

[NaCl] (M)	tan δ (–)	
	min	max
0.3	0.19	0.34
0.6	0.12	0.15
0.75	0.08	0.11

hydrophobic interactions. The tangent of the phase angle, tan δ = *G''/G'*, Table 1, decreases with increasing salt and shows that more elastic materials are obtained with increasing salt concentration [40]. The TERPOCs can be compared to gels of $NIPAM_{455}$-*b*-DMA_{210}-*b*-$NIPAM_{455}$ or $NIPAM_{320}$-*b*-$HEMA_{80}$-*b*-$NIPAM_{320}$ which contain hydrophilic centre blocks instead of a polyelectrolyte block which is complexed with an oppositely charged polymer. Higher *G'* are observed for TERPOCs at 50 °C, while lower polymer concentrations are used, compared to the uncomplexed gels [38,41]. Consequently, polyelectrolyte complexes contribute to the stiffness of temperature-responsive polymer gels by creating additional electrostatic cross-links.

Shear start-up. At 50 °C, shear start-up experiments are performed to determine the non-linear rheological behaviour of the gel. Initially, the stress increases and subsequently drops sharply, indicating fracture of the gel, Fig. 7A. Comparison of the peak stresses shows no significant difference between the samples. However, a small trend can be observed when the peak strains are compared and an optimum is observed at 0.6 M NaCl, Fig. 7B. This optimum may be explained by the dependence of electrostatic interactions on the salt concentration. During deformation, electrostatic bonds break, but may also reform. The relaxation time of the electrostatic bonds decreases with increasing salt, therefore, at 0.3 M NaCl, the ruptured bonds may not be restored timely and the stress-strain peak is observed at lower strain. At 0.6 M NaCl, on the other hand, shorter relaxation times lead to a faster reformation of the electrostatic interactions which increases the peak strain. At 0.75 M NaCl, the strain decreases again because the increased salt concentration limits the solubility and thus the mobility of the PNIPAM chains. Consequently, PNIPAM node formation is hindered, which leads to a lower peak strain. Again, it is shown that the properties are a result of the balance between the electrostatic and hydrophobic interactions, which can be tuned with the salt concentration.

Frequency sweep. Fig. 7C shows the frequency dependence of the storage and loss modulus in which different behaviours are observed. The sample with 0.3 M NaCl shows frequency-dependent behaviour indicating viscoelasticity. At 0.6 M NaCl, a critical gel seems to be found, which is an intermediate state between liquid and solid. Critical gels are characterized by a power law relation with scaling *n* between the moduli and frequency, and by a constant tan δ which is determined as $\tan(n\pi/2)$ (Fig. S9) [42]. The sample at 0.6 M NaCl is highly physically cross-linked, as indicated by the low $n \approx 0.09$. Finally, the sample at 0.75 M NaCl, behaves like an elastic solid, which is characterized by a constant modulus with changing frequency [35]. At 0.75 M, the NaCl concentration has severely reduced the contribution of the complex coacervates. Consequently, the frequency-independent behaviour is mainly caused by the PNIPAM interactions, while the frequency dependence is mainly caused by the electrostatic interactions.

3.3.2. Effects of charge compensation

The amount of PDMAEMA is lowered to investigate the effect of incomplete charge neutralization of the PAA at 0.3 M NaCl. When PDMAEMA is absent, the material hardly strengthens, Fig. 8A, and the final material is so weak that the torque, ≈ 2 nNm to ≈ 7 nNm, does not exceed the detection limit. Therefore, either complexation with a polycation or a higher polymer concentration is required to obtain stable gels with PNIPAM-*b*-PAA-*b*-PNIPAM at pH 6.5.

Stable gelation occurred when half of the anionic charges were compensated by PDMAEMA, Fig. 8B. Nevertheless, the moduli at 50 °C are an order of magnitude lower compared to charge-neutral samples. This effect may be caused by a slightly lower polymer concentration, and by fewer electrostatic interactions with the same amount of salt, leading to shorter relaxation times of the electrostatic interactions. Nevertheless, at 0.3 M NaCl, more charge compensation than 50% is needed to reach an optimum amount of crosslinks. Furthermore, the stress-strain curves look slightly different and the peak strain is somewhat higher when only half of the charges are neutralised, Fig. 8C. This may be explained by a higher chance to reform ruptured bonds, as anionic charges are always available. Moreover, the frequency-dependent behaviour is comparable, Fig. 8D, while tan δ is lowered for the charged TERPOC. A lower tan δ value can be caused by a higher relative PNIPAM content which results in a slightly more elastic material. Overall, charge compensation is required to obtain strong gels at this salt concentration, and can be used to adjust the properties of TERPOCs.

3.3.3. Polymer concentration dependence

The effects of the polymer concentration on the properties of the TERPOCs was investigated at 0.3 M NaCl, Fig. 9A. In accordance with literature, a decreasing T_{gel} with increasing polymer concentration is observed. This effect can be ascribed to a higher probability of polymers to entangle when the concentration increases, which causes a lower LCST and thus a lower T_{gel} [37,43–45,38]. An increase in storage modulus is found when the polymer concentration is increased from 4 to 7.5 wt%. This trend can be explained by an increasing number of (PNIPAM) nodes because of the higher polymer concentration, resulting

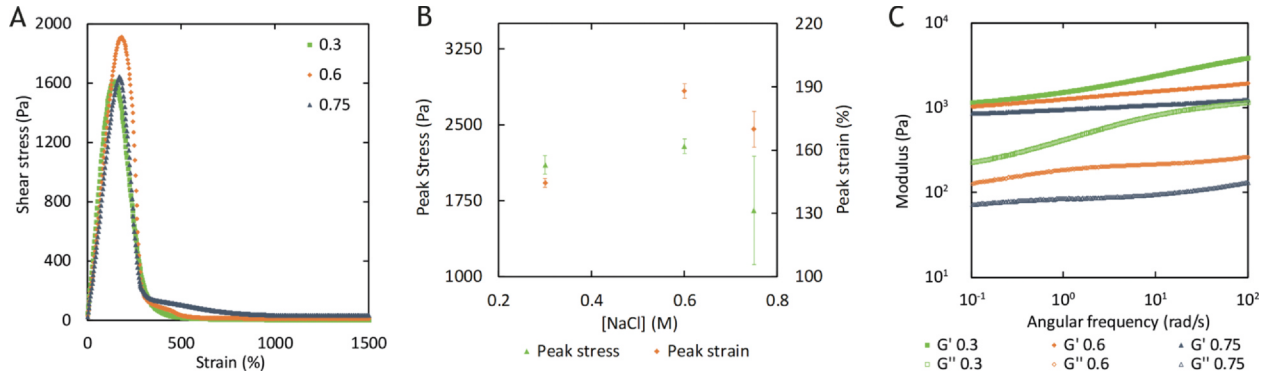

Fig. 7. A Shear stress as function of strain, **B** overview of average peak stress and strain, and **C** storage and loss modulus as function of angular frequency, for varying NaCl concentrations (M) at 7.5 wt% polymer and 50 °C. The error bars depicted in B show the standard deviations. For 0.3 M NaCl three samples were measured, whereas for 0.6 and 0.75 M NaCl two samples were measured. Quantitative data is provided in Table S2.

in a higher storage modulus. Also, the dissipation of energy increases when polymers get closer, causing a higher loss modulus. However, a surprisingly small difference is observed between 7.5 and 10 wt% polymer. The approximately equal moduli indicate that the number of nodes did not increase with the polymer concentration. A possible explanation can be that the higher PNIPAM concentration causes a faster gelation. Therefore, equilibration of the sample is hindered and node formation may be obstructed.

In the shear start-up experiments, Fig. 9B, the peak strain and stress increase strongly with concentration. Previously, it has been found that the relation between the polymer concentration and material strength shows an optimum [21]. An increasing polymer concentration causes improved stiffness and energy dissipation at first, which increases the peak strain and stress. However, when the optimum is passed, the viscoelastic properties turn into elastic behaviour, which lowers the resistance to interfacial crack propagation and therewith the peak strain. Since we have not observed an optimum, the optimal polymer concentration for this TERPOC is expected to be 10 wt% or more. Furthermore, the frequency dependence of the moduli, Fig. 9C, is similar for all polymer concentrations, because of the constant salt concentration. In addition, tan δ becomes less frequency-dependent upon increasing the polymer concentration, Fig. S9B, which shows that the material becomes more elastic at higher concentrations.

3.3.4. Optimal conditions

Both the sample with 0.6 M NaCl and 7.5 wt%, and the sample with 0.3 M NaCl and 10 wt% showed an optimum performance in the stress-strain curves. To determine whether the material properties can be

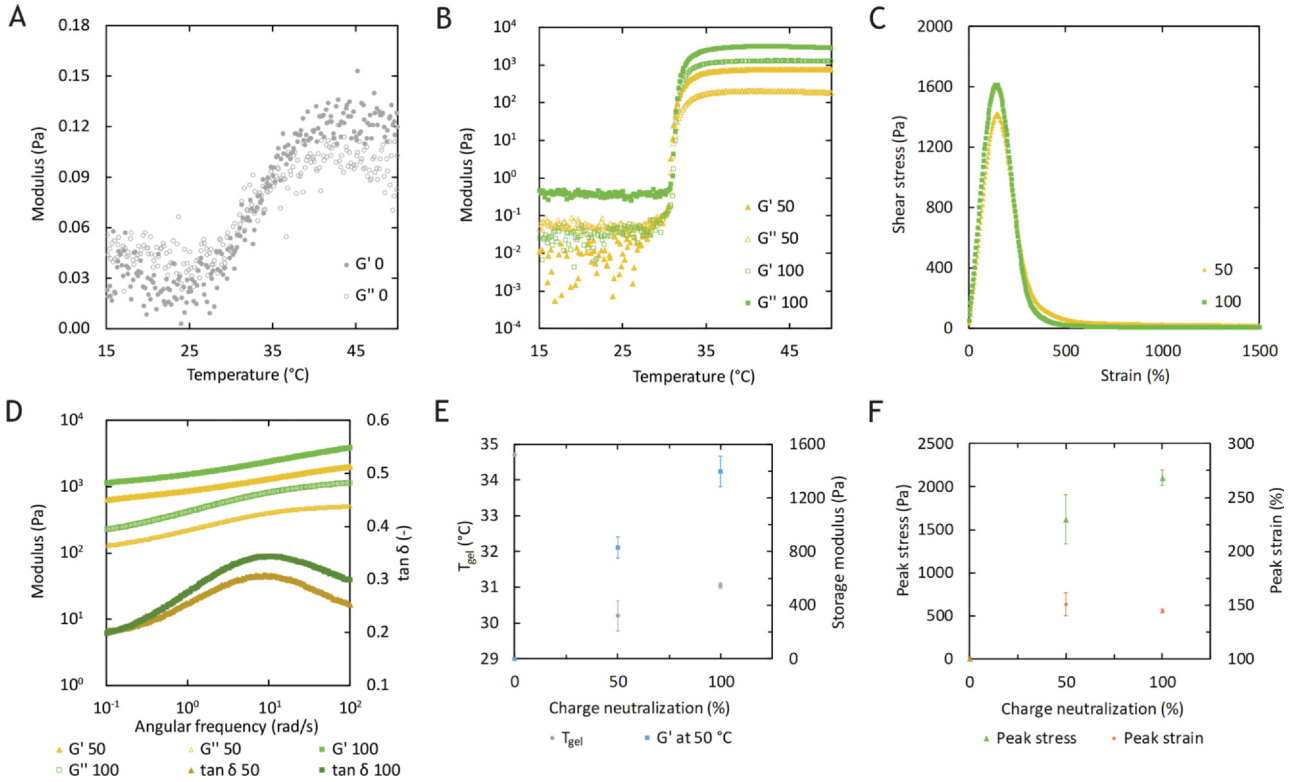

Fig. 8. A Storage and loss moduli are shown as a function of temperature for 6 wt% PNIPAM-*b*-PAA-*b*-PNIPAM at 0.3 M NaCl (no PDMAEMA). The torque increased from ≈2 nNm till ≈7 nNm, which is in any case below the detection limit. **B** Storage and loss moduli are shown as a function of temperature for 0.3 M NaCl and PDMAEMA to compensate half (50) (c_{pol} 6.75 wt%) or all (100) (c_{pol} 7.5 wt%) of the anionic charges. **C** The shear stress as function of rotational strain and **D** the frequency-dependent behaviour of the moduli and tan δ, for the same samples. The results of the **E** temperature sweep and **F** stress-strain curves have been averaged for two measurements and are depicted with the standard deviations. For the sample without PDMAEMA only one sample was measured.

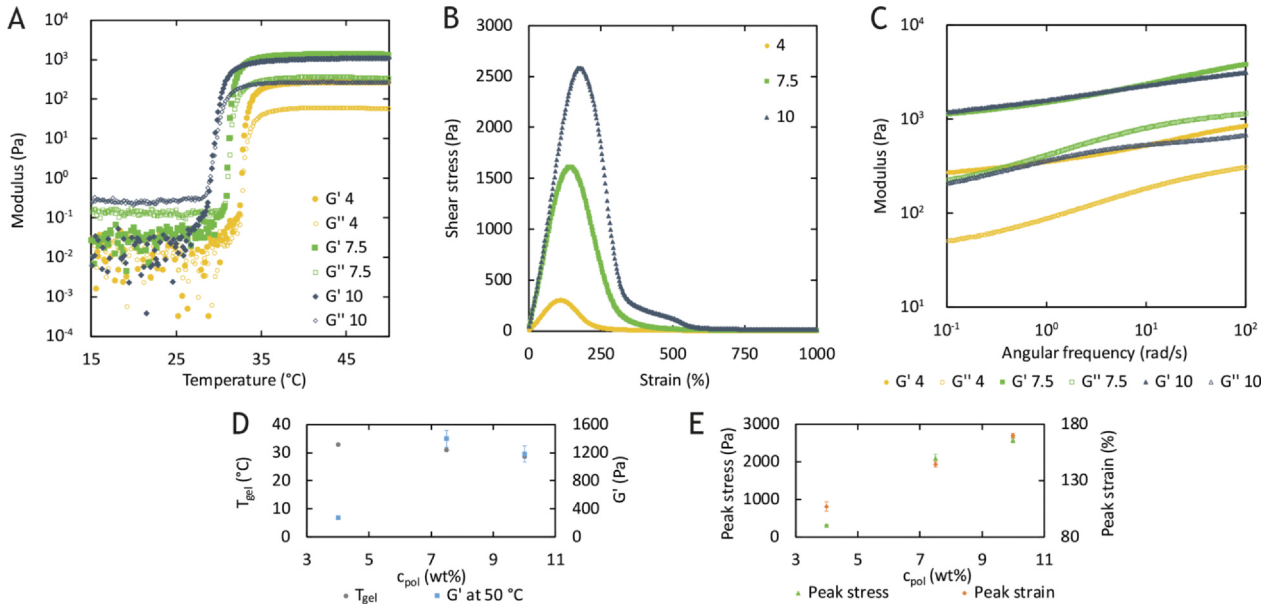

Fig. 9. A Storage and loss moduli as function of temperature for 0.3 M NaCl and varying polymer concentrations (wt%). **B** Shear stress as function of strain, and **C** storage and loss modulus as function of angular frequency, at 50 °C, are shown for the same samples. **D** Average T_{gel} and storage modulus, as obtained at 50 °C before equilibration, as function of polymer concentration, c_{pol}. **E** Overview of average peak stress and strain, at varying polymer concentrations. The error bars indicate the standard deviation. For 7.5 wt% three samples were measured, whereas for 4 and 10 wt% two samples were measured.

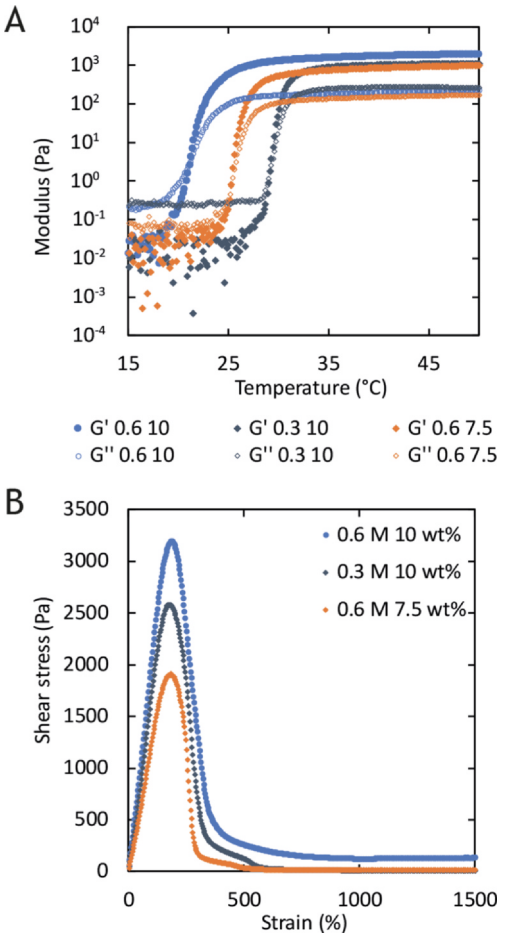

Fig. 10. A Storage and loss moduli as function of temperature, for different NaCl (M) and polymer (wt%) concentrations. **B** Shear stress as function of strain at 50 °C for the same samples.

further enhanced, a sample with 0.6 M NaCl and 10 wt% polymer is investigated. For this sample, T_{gel} decreases even further while G' increases and G'' is hardly affected, Fig. 10A. The decreasing T_{gel} can be explained by a lower LCST and a higher probability of cross-linking through the increased polymer concentration. Moreover, a higher salt concentration reduces T_{gel} as well. Furthermore, an increased polymer concentration may lead to a higher number of nodes, causing a higher G'. This change in G' is observed at 0.6 M NaCl, but at 0.3 M NaCl no effects are observed. This difference can be explained by the amount of salt that is needed to create sufficient mobility of the polyelectrolyte chains to equilibrate the TERPOC and create an optimal number of nodes, leading to a higher G'. Moreover, the sample with 0.75 M NaCl and 10 wt% polymer, shows a higher peak stress in the stress-strain curve, Fig. 10B, while the strain for this sample is not further increased. Therefore, we can conclude that increasing both the salt and polymer concentration creates a stronger material. Also, the sample at 0.6 M NaCl and 7.5 wt% looks like a critical gel as the moduli increase with frequency, while tan δ remains constant, Fig. S10. This confirms that the salt concentration alters the frequency response, while the polymer concentration does not.

Dompé et al. recently investigated comparable TERPOCs of PAA and poly(dimethylaminopropyl acrylamide) grafted with 30% PNIPAM in NaCl solutions. Compared to their work, this system shows a lower cross-over temperature, and the moduli are an order of magnitude higher [12]. Both of these observations can be explained by the higher polymer concentration and also by the higher PNIPAM content of ≈ 70 wt%. A higher polymer concentration is known to decrease the LCST of PNIPAM. Moreover, higher PNIPAM concentrations enhance the formation of hydrophobic interactions, which lowers the LCST and increases the cross-linking density in the solid PNIPAM phase. The values found for tan δ, and the dependence of the moduli on the angular frequency are similar, which suggests comparable elasticity of the materials. However, the peak stress in materials with 70 wt% PNIPAM has increased tremendously, while the peak strain has decreased. This shows that the material with 70 wt% PNIPAM can withstand higher loads, but is less extensible as it breaks at lower deformations.

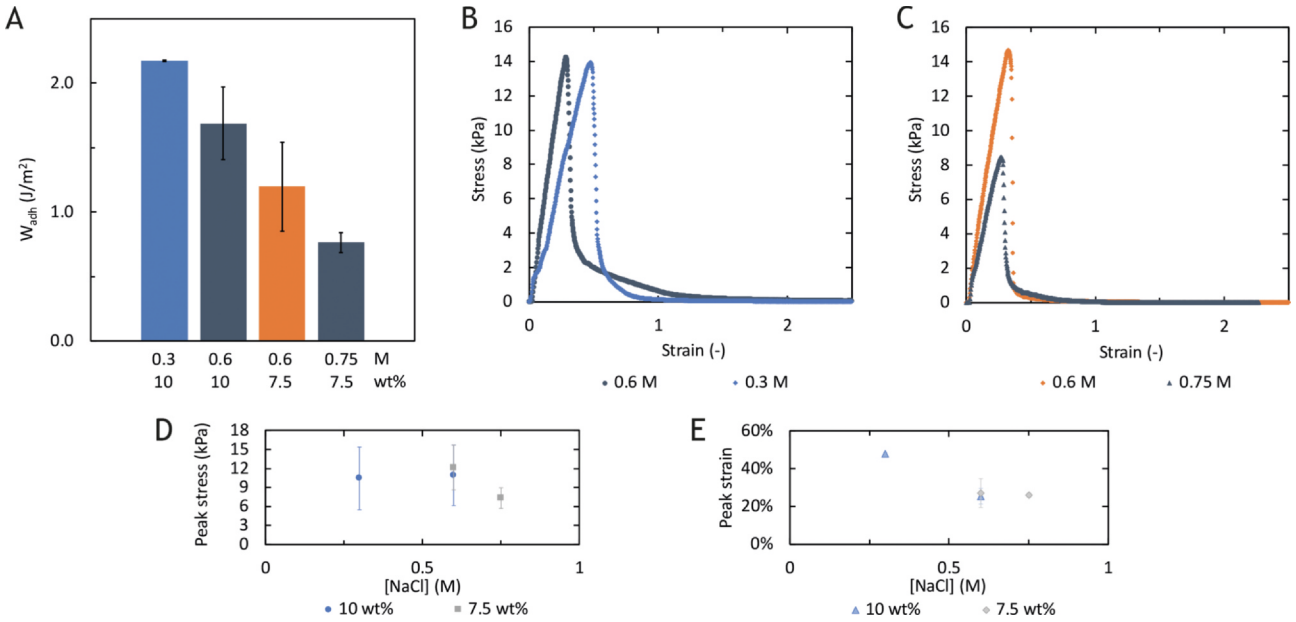

Fig. 11. A Work of adhesion for four different samples containing 71 wt% PNIPAM and varying NaCl (M) and polymer concentrations (wt%) at 50 °C. Average peak **B** stress and **C** strain values with their standard deviations as calculated from two representative measurements. Typical stress-strain curves for varying NaCl concentrations and **D** 10 wt% or **E** 7.5 wt% polymer.

3.4. Probe tack testing

Probe tack experiments are performed to determine the adhesive strength of the TERPOCs. The samples are applied onto a glass slide and contact was made, followed by a sudden increase in temperature till 50 °C, by pouring a heated salt solution into the chamber. The salt concentration of the solution is equal to the salt concentration of the sample, to investigate the temperature-responsive curing only. Moreover, adhesive performance depends on the type of substrate and glass was selected as a proof of principle.

Two clear trends can be observed in the data, Fig. 11A. First, higher polymer concentrations lead to a higher work of adhesion, W_{adh}. This can be explained by an increased amount of adhesive and cohesive bonds that have to be broken, before rupture of the adhesive occurs. Secondly, lower salt concentrations lead to an increased W_{adh}. This can be caused by the improved strength of the electrostatic interactions. It is was shown that curing of the adhesive caused by a salt-switch leads to an improved W_{adh}. Therefrom it can be concluded that lower salt concentrations lead to a better W_{adh}, which is also observed in this work [13].

An optimal work of adhesion (W_{adh}) of 2.2 J/m^2 was obtained for PNIPAM-rich TERPOCs submerged in saline solutions. However, a higher W_{adh} of 3.8 J/m^2 was previously found for grafted polyelectrolytes that contained a smaller amount of PNIPAM, likely due to the lower brittleness and lower water content. More specifically, extrusion was shown to be an effective method for increasing the W_{adh} and would also be an interesting method to further improve the adhesion of the TERPOCs described in this work [21]. Nevertheless, the maximum observed W_{adh} is significantly stronger than the negligible adhesive strength reported for commonly used pressure-sensitive adhesives (PSA), where only one drop of seawater was present [46]. Furthermore, for other biomimetic underwater adhesives, values between 0.003 and 75 J/m^2 are reported [46,12]. Most of these materials are based on catechol chemistry, or require a chemical reaction to solidify, while TERPOCs set easily and safely by simply changing the temperature. Therefore, TERPOCs are a suitable and simple material for developing underwater adhesives.

3.5. Sample stability

The distinct temperature treatment in rheology and probe tack testing leads to different observations when the data is compared. With the probe tack test, a higher peak strain is observed for 0.3 M NaCl than for 0.6 M NaCl at 10 wt%, while the opposite is found with rheology, Fig. 11B and Fig. 10B. A first explanation is the T_{gel} of 0.6 M NaCl, which is about 21 °C. Consequently, in probe tack testing, gelation can occur before making contact with the glass substrate. While in rheology, the sample is cooled to 10 °C which ensures a liquid state at the start of the measurement. The different phases of the TERPOCs at the beginning of the measurement result in the contradicting tendencies and underline the importance of sample history. Moreover, a second explanation can be found in the speed of the temperature change. In rheology, the temperature increases slowly, which allows sufficient time for the TERPOC to equilibrate and a obtain a stable hydrogel. In the probe tack test, however, the sample is heated suddenly, which causes a different polymer morphology and the sample cracked within a few minutes. This instability coincides with observations from a preliminary experiment in which samples with 0.5 M NaCl and different polymer concentrations (1, 3, 5, 7.5 and 10 wt%) were placed in an oven at 50 °C. All samples showed syneresis, i.e. they expelled water, and the 10 wt% sample fractured spontaneously after multiple hours. These observations show that the amount of PNIPAM is too high to embed the water inside the polyelectrolyte domains of the TERPOC, leading to unstable samples. Therefore, it would be interesting to investigate whether lowering the water content improves the stability of the TERPOC and thus creates materials closer to equilibrium. Reducing the amount of water by extrusion, for example, enhances the adhesive performance as was recently shown by Dompé et al. [21]. On top of that, lowering the PNIPAM content will also increase the amount of water in the sample, which will improve the stability. This adjustment requires the synthesis of new block copolymers, as is shown in the supplementary information, Fig. S11. Overall, we believe that TERPOCs are promising materials for the development of underwater adhesives.

4. Conclusion

Temperature-responsive polyelectrolytes were used to prepare

PNIPAM-rich TERPOCs for underwater adhesion. Upon heating, the C3M solution forms a gel, resulting in strong, but somewhat brittle TERPOCs because of the high PNIPAM content. Moreover, the polyelectrolytes enhance gelation and improve the strength of the gel. In addition, charge neutralization by PDMAEMA is required to obtain strong gels. However, excess charge seems to result in a slightly better extensibility. Furthermore, the properties of the TERPOCs could be tuned by varying the salt and polymer concentration. Less salt increases T_{gel} which alters the morphology of the TERPOC and reduces its water content, leading to better adhesion. Nevertheless, the amount of PNIPAM in these TERPOCs leads to unstable hydrogels due to water release. Therefore, further research is needed to find the optimal PNIPAM content to fully exploit the suitability and simplicity of TERPOCs as underwater adhesives.

Data availability statement

The raw/processed data required to reproduce these findings cannot be shared at this time due to technical or time limitations.

Declaration of Competing Interest

The authors declare that they have no known competing financial interests or personal relationships that could have appeared to influence the work reported in this paper.

Acknowledgements

SAXS measurements were performed at the Dutch Belgium beamline of the ESRF in Grenoble, with experimental assistance of Michela Brunelli, Daniel Hermida Merino and Remco Fokkink. Mehdi Vahditi is thanked for help with the probe tack experiments at the ESPCI in Paris. Sjoerd Verboom is acknowledged for the synthesis of the PNIPAM homopolymer and its RAFT agent. Wouter Teunissen is acknowledged for performing GPC measurements. This research was financially supported by an NWO VIDI grant.

Appendix A. Supplementary material

Supplementary data associated with this article can be found, in the online version, at https://doi.org/10.1016/j.eurpolymj.2020.110034.

References

[1] J.H. Waite, Natures underwater adhesive specialist, Chemtech 17 (11) (1987) 692–697 URL < Go to ISI > ://WOS:A1987L400300012.
[2] A.H. Hofman, I.A. van Hees, J. Yang, M. Kamperman, Bioinspired underwater adhesives by using the supramolecular toolbox, Adv. Mater. 30 (19) (2018) 1704640, https://doi.org/10.1002/adma.201704640 URL < Go to ISI > ://WOS:000431616700011.
[3] M. Tekaat, D. Butergerds, M. Schonhoff, A. Fery, C. Cramer, Scaling properties of the shear modulus of polyelectrolyte complex coacervates: a time-ph superposition principle, PCCP 17 (35) (2015) 22552–22556, https://doi.org/10.1039/c5cp02940f URL < Go to ISI > ://WOS:000360448300010.
[4] E. Spruijt, M.A.C. Stuart, J. van der Gucht, Linear viscoelasticity of polyelectrolyte complex coacervates, Macromolecules 46 (4) (2013) 1633–1641, https://doi.org/10.1021/ma301730n URL < Go to ISI > ://WOS:000315618800043.
[5] T. Akagi, K. Watanabe, H. Kim, M. Akashi, Stabilization of polyion complex nanoparticles composed of poly(amino acid) using hydrophobic interactions, Langmuir 26 (4) (2010) 2406–2413, https://doi.org/10.1021/la902868g URL < Go to ISI > ://WOS:000274342200035.
[6] E. Spruijt, A.H. Westphal, J.W. Borst, M.A.C. Stuart, J. van der Gucht, Binodal compositions of polyeleetrolyte complexes, Macromolecules 43 (15) (2010) 6476–6484, https://doi.org/10.1021/ma101031t URL < Go to ISI > ://WOS:000280743300031.
[7] Y. Lee, C.J. Xu, M. Sebastin, A. Lee, N. Holwell, C.V. Xu, D.M. Nieves, L.Y. Mu, R.S. Langer, C.P. Lin, J.M. Karp, Bioinspired nanoparticulate medical glues for minimally invasive tissue repair, Adv. Healthcare Mater. 4 (16) (2015) 2587–2596, https://doi.org/10.1002/adhm.201500419 URL < Go to ISI > ://WOS:000368142100016 https://onlinelibrary.wiley.com/doi/pdf/10.1002/adhm.201500419.
[8] A.H. Hofman, R. Fokkink, M. Kamperman, A mild and quantitative route towards well-defined strong anionic/hydrophobic diblock copolymers: synthesis and aqueous self-assembly, Polym. Chem. 10 (2019) 6109–6115, https://doi.org/10.1039/C9PY01227C.
[9] M.A. Ward, T.K. Georgiou, Thermoresponsive polymers for biomedical applications, Polymers 3 (3) (2011) 1215–1242, https://doi.org/10.3390/polym3031215 URL < Go to ISI > ://WOS:000208601700016.
[10] H.G. Schild, Poly (n-isopropylacrylamide) - experiment, theory and application, Prog. Polym. Sci. 17 (2) (1992) 163–249, https://doi.org/10.1016/0079-6700(92)90023-R URL < Go to ISI > ://WOS:A1992HZ36200001.
[11] T. Patel, G. Ghosh, S. Yusa, P. Bahadur, Solution behavior of poly(N-isopropylacrylamide) in water: Effect of additives, J. Dispersion Sci. Technol. 32 (8) (2011) 1111–1118, https://doi.org/10.1080/01932691.2010.497701 URL ://WOS:000295219200006.
[12] M. Dompé, F.J. Cedano-Serrano, O. Heckert, N. van den Heuvel, J. Van der Gucht, Y. Tran, D. Hourdet, C. Creton, M. Kamperman, Thermoresponsive complex coacervate-based underwater adhesive, Adv. Mater. (2019) 1808179.
[13] M. Dompé, F.J. Cedano-Serrano, M. Vahdati, L. van Westerveld, D. Hourdet, C. Creton, J. van der Gucht, T. Kodger, M. Kamperman, Underwater adhesion of multiresponsive complex coacervates, Adv. Mater. Interfaces (2019) 1901785, https://doi.org/10.1002/admi.201901785.
[14] M. Dompé, F.J. Cedano-Serrano, M. Vahdati, U. Sidoli, O. Heckert, A. Synytska, D. Hourdet, C. Creton, J. van der Gucht, T. Kodger, M. Kamperman, Tuning the interactions in multiresponsive complex coacervate-based underwater adhesives, Int. J. Mol. Sci. 21 (100). doi:10.3390/ijms21010100.
[15] E. Spruijt, J. Sprakel, M. Lemmers, M.A.C. Stuart, J. van der Gucht, Relaxation dynamics at different time scales in electrostatic complexes: Time-salt superposition, Phys. Rev. Lett. 105(20). doi:ARTN 208301 10.1103/PhysRevLett.105.208301. URL < Go to ISI > ://WOS:000283927700010 https://journals.aps.org/prl/pdf/10.1103/PhysRevLett.105.208301.
[16] J. van der Gucht, E. Spruijt, M. Lemmers, M.A.C. Stuart, Polyelectrolyte complexes: Bulk phases and colloidal systems, J. Colloid Interface Sci. 361 (2) (2011) 407–422, https://doi.org/10.1016/j.jcis.2011.05.080 URL < Go to ISI > ://WOS:000293038200001.
[17] N. Lang, M.J. Pereira, Y. Lee, I. Friehs, N.V. Vasilyev, E.N. Feins, K. Ablasser, E.D. O'Cearbhaill, C. Xu, A. Fabozzo, R. Padera, S. Wasserman, F. Freudenthal, L.S. Ferreira, R. Langer, J.M. Karp, P.J.A. del Nido, Blood-resistant surgical glue for minimally invasive repair of vessels and heart defects, Sci. Translational Med. 6 (218) (2014) 218ra6, https://doi.org/10.1126/scitranslmed.3006557.
[18] C.L.E. Nijst, J.P. Bruggeman, J.M. Karp, L. Ferreira, A. Zumbuehl, C.J. Bettinger, R. Langer, Synthesis and characterization of photocurable elastomers from poly (glycerol-co-sebacate), Biomacromolecules 8 (10) (2007) 3067–3073, https://doi.org/10.1021/bm070423u.
[19] B. Ahn, S. Das, R. Linstadt, Y. Kaufman, N.R. Martinez-Rodriguez, R. Mirshafian, E. Kesselman, Y. Talmon, B.H. Lipshutz, J.N. Israelachvili, J.H. Waite, High-performance mussel-inspired adhesives of reduced complexity, Nat. Commun. 6 (2015) 8663, https://doi.org/10.1038/ncomms9663.
[20] S. Seo, S. Das, P.J. Zalicki, R. Mirshafian, C.D. Eisenbach, J.N. Israelachvili, J.H. Waite, B.K. Ahn, Microphase behavior and enhanced wet-cohesion of synthetic copolyampholytes inspired by a mussel foot protein, J. Am. Chem. Soc. 137 (29) (2015) 9214–9217, https://doi.org/10.1021/jacs.5b03827.
[21] M. Dompé, M. Vahdati, F. van Ligten, F.J. Cedano-Serrano, D. Hourdet, C. Creton, M. Zanetti, P. Bracco, J. van der Gucht, T. Kodger, M. Kamperman, Enhancement of the adhesive properties by optimizing the water content in pnipam-functionalized complex coacervates, ACS Appl. Polym. Mater. 2 (4) (2020) 1722–1730, https://doi.org/10.1021/acsapm.0c00185.
[22] M. Dompé, F.J. Cedano-Serrano, M. Vahdati, D. Hourdet, J. van der Gucht, M. Kamperman, T. Kodger, Hybrid complex coacervate, Polymers 12 (2) (2020) 320, https://doi.org/10.3390/polym12020320.
[23] C. Wei, X. Zhu, H. Peng, J. Chen, F. Zhang, Q. Zhao, Facile preparation of lignin-based underwater adhesives with improved performances, ACS Sustain. Chem. Eng. 7 (4) (2019) 4508–4514, https://doi.org/10.1021/acssuschemeng.8b06731.
[24] I.A. Van Hees, P.J.M. Swinkels, R.G. Fokkink, A.H. Velders, I.K. Voets, J. Van der Gucht, M. Kamperman, Self-assembly of oppositely charged polyelectrolyte block copolymers containing short thermoresponsive blocks, Polym. Chem. 10 (2019) 3127–3134.
[25] B. Fehér, K. Zhu, B. Nyström, I. Varga, J.S. Pedersen, Effect of temperature and ionic strength on micellar aggregates of oppositely charged thermoresponsive block copolymer polyelectrolytes, Langmuir 35 (2019) 13614–13623, https://doi.org/10.1021/acs.langmuir.9b01896.
[26] A.M. Bivigou-Koumba, J. Kristen, A. Laschewsky, P. Muller-Buschbaum, C.M. Papadakis, Synthesis of symmetrical triblock copolymers of styrene and n-isopropylacrylamide using bifunctional bis(trithiocarbonate)s as raft agents, Macromol. Chem. Phys. 210 (7) (2009) 565–578, https://doi.org/10.1002/macp.200800575 URL < Go to ISI > ://WOS:000265322100007.
[27] A.D. Filippov, I.A. van Hees, R. Fokkink, I.K. Voets, M. Kamperman, Rapid and quantitative de-tert-butylation for poly(acrylic acid) block copolymers and influence on relaxation of thermoassociated transient networks, Macromolecules 51 (20) (2018) 8316–8323, https://doi.org/10.1021/acs.macromol.8b01440 URL < Go to ISI > ://WOS:000448753000041.
[28] M. Borsboom, W. Bras, I. Cerjak, D. Detollenaere, D.G. van Loon, P. Goedtkindt, M. Konijnenburg, P. Lassing, Y.K. Levine, B. Munneke, M. Oversluizen, R. van Tol, E. Vlieg, The dutch-belgian beamline at the esrf, J. Synchrotron Radiat. 5 (1998) 518–520, https://doi.org/10.1107/S0909049597013484 URL < Go to ISI > ://WOS:000074975200100.
[29] W. Bras, I.P. Dolbnya, D. Detollenaere, R. van Tol, M. Malfois, G.N. Greaves, A.J. Ryan, E. Heeley, Recent experiments on a combined small-angle/wide-angle x-

ray scattering beam line at the esrf, J. Appl. Crystallogr. 36 (2003) 791–794, https://doi.org/10.1107/S0021889803004000x URL < Go to ISI > :// WOS:000182284400088.
[30] M. Schwab, B. Stuhn, Thermotropic transition from a state of liquid order to a macrolattice in asymmetric diblock copolymers, Phys. Rev. Lett. 76 (6) (1996) 924–927, https://doi.org/10.1103/PhysRevLett.76.924 URL < Go to ISI > :// WOS:A1996TT49100018.
[31] G.A. Mcconnell, A.P. Gast, J.S. Huang, S.D. Smith, Disorder-order transitions in soft-sphere polymer micelles, Phys. Rev. Lett. 71 (13) (1993) 2102–2105, https://doi.org/10.1103/PhysRevLett.71.2102 URL < Go to ISI > ://WOS:A1993LZ39100036.
[32] A.H. Hofman, G. ten Brinke, K. Loos, Asymmetric supramolecular double-comb diblock copolymers: From plasticization, to confined crystallization, to breakout, Polymer 121 (2017) 312–319, https://doi.org/10.1016/j.polymer.2017.05.057.
[33] T. Lopez-Leon, A. Fernandez-Nieves, Macroscopically probing the entropic influence of ions: Deswelling neutral microgels with salt, Physical Review E 75 (1). doi:ARTN 011801 10.1103/PhysRevE.75.011801. URL < Go to ISI > :// WOS:000243893400073.
[34] B. Sierra-Martin, Y. Laporte, A.B. South, L.A. Lyon, A. Fernandez-Nieves, Bulk modulus of poly(n-isopropylacrylamide) microgels through the swelling transition, Phys. Rev. E 84 (1). doi:ARTN 011406 10.1103/PhysRevE.84.011406. URL < Go to ISI > ://WOS:000293455900005.
[35] J.H. Laurer, J.F. Mulling, S.A. Khan, R.J. Spontak, J.S. Lin, R. Bukovnik, Thermoplastic elastomer gels. ii. effects of composition and temperature on morphology and gel rheology, J. Polym. Sci. Part B-Polym. Phys. 36 (14) (1998) 2513–2523 URL < Go to ISI > ://WOS:000076115700005.
[36] K. Mortensen, Structural properties of self-assembled polymeric micelles, Curr. Opin. Colloid Interface Sci. 3 (1) (1998) 12–19, https://doi.org/10.1016/S1359-0294(98)80036-8 URL < Go to ISI > ://WOS:000072452500003.
[37] N. Beheshti, K.Z. Zhu, A.L. Kjoniksen, K.D. Knudsen, B. Nystrom, Characterization of temperature-induced association in aqueous solutions of charged ABCBA-type pentablock tercopolymers, Soft Matter 7 (3) (2011) 1168–1175, https://doi.org/10.1039/c0sm00892c URL ://WOS:000286615500049.
[38] S.E. Kirkland, R.M. Hensarling, S.D. McConaughy, Y. Guo, W.L. Jarrett, C.L. McCormick, Thermoreversible hydrogels from RAFT-synthesized BAB triblock copolymers: Steps toward biomimetic matrices for tissue regeneration, Biomacromolecules 9 (2) (2008) 481–486, https://doi.org/10.1021/bm700968t URL ://WOS:000253102100009.
[39] Y.J. Zhang, S. Furyk, D.E. Bergbreiter, P.S. Cremer, Specific ion effects on the water solubility of macromolecules: Pnipam and the hofmeister series, J. Am. Chem. Soc. 127 (41) (2005) 14505–14510, https://doi.org/10.1021/ja0546424 URL < Go to ISI > ://WOS:000232605600076.
[40] K.J. Krzyminski, M. Jasionowski, A. Gutowska, Reversible sol-gel transitions in aqueous solutions of n-isopropylacrylamide ionic copolymers, Polym. Int. 57 (4) (2008) 592–604, https://doi.org/10.1002/pi.2318 URL < Go to ISI > :// WOS:000254688800006.
[41] X.L. Zhao, W.G. Liu, D.Y. Chen, X.Z. Lin, W.W. Lu, Effect of block order of ABA- and BAB-type NIPAAm/HEMA triblock copolymers on thermoresponsive behavior of solutions, Macromol. Chem. Phys. 208 (16) (2007) 1773–1781, https://doi.org/10.1002/macp.200700155 URL ://WOS:000249050000007.
[42] T. Vermonden, N.A.M. Besseling, M.J. van Steenbergen, W.E. Hennink, Rheological studies of thermosensitive triblock copolymer hydrogels, Langmuir 22 (24) (2006) 10180–10184, https://doi.org/10.1021/la062224m URL < Go to ISI > :// WOS:000242022100057.
[43] C. Chassenieux, T. Nicolai, L. Benyahia, Rheology of associative polymer solutions, Curr. Opinion Colloid Interface Sci. 16 (1) (2011) 18–26, https://doi.org/10.1016/j.cocis.2010.07.007 URL < Go to ISI > ://WOS:000287563300004.
[44] L. Despax, J. Fitremann, M. Destarac, S. Harrisson, Low concentration thermoresponsive hydrogels from readily accessible triblock copolymers, Polym. Chem. 7 (20) (2016) 3375–3377, https://doi.org/10.1039/c6py00499g URL < Go to ISI > ://WOS:000376090400003.
[45] S. Kirkland-York, K. Gallow, J. Ray, Y.L. Loo, C. McCormick, Temperature-induced ordering and gelation of star micelles based on ABA triblocks synthesized via aqueous RAFT polymerization, Soft Matter 5 (11) (2009) 2179–2182, https://doi.org/10.1039/b823131a URL ://WOS:000266371400004.
[46] S.K. Clancy, A. Sodano, D.J. Cunningham, S.S. Huang, P.J. Zalicki, S. Shin, B.K. Ahn, Marine bioinspired underwater contact adhesion, Biomacromolecules 17 (5) (2016) 1869–1874, https://doi.org/10.1021/acs.biomac.6b00300 URL < Go to ISI > ://WOS:000375886500033.
[47] D.G. Lessard, M. Ousalem, X.X. Zhu, A. Eisenberg, P.J. Carreau, Study of the phase transition of poly(N,N-diethylacrylamide) in water by rheology and dynamic light scattering, J. Polym. Sci. Part B-Polym. Phys. 41 (14) (2003) 1627–1637, https://doi.org/10.1002/polb.10517 URL ://WOS:000183812400004.
[48] C. Tsitsilianis, G. Serras, C.H. Ko, F. Jung, C.M. Papadakis, M. Rikkou-Kalourkoti, C.S. Patricicios, R. Schweins, C. Chassenieux, Thermoresponsive hydrogels based on telechelic polyelectrolytes: From dynamic to frozen networks, Macromolecules 51 (6) (2018) 2169–2179, https://doi.org/10.1021/acs.macromol.8b00193 URL < Go to ISI > ://WOS:000428712300003.
[49] H. Guo, N. Sanson, D. Hourdet, A. Marcellan, Thermoresponsive toughening with crack bifurcation in phase-separated hydrogels under isochoric conditions, Adv. Mater. 28 (2016) 5857–5864, https://doi.org/10.1002/adma.201600514.
[50] S. Bayati, K.E. Bergquist, K.Z. Zhu, B. Nystrom, J.S. Pedersen, L. Galantini, K. Schillen, Mixed micelles of oppositely charged poly(N-isopropylacrylamide) diblock copolymers, J. Polym. Sci. Part B-Polym. Phys. 55 (19) (2017) 1457–1469, https://doi.org/10.1002/polb.24403 URL ://WOS:000407842600004.